In vitro reconstitution of SARS-CoV-2 Nsp1-induced mRNA cleavage reveals the key roles of the N-terminal domain of Nsp1 and the RRM domain of eIF3g

Irina S. Abaeva,[1] Yani Arhab,[1] Anna Mińcicka, Christopher U.T. Hellen, and Tatyana V. Pestova

Department of Cell Biology, State University of New York Downstate Health Sciences University, Brooklyn, New York 11203, USA

SARS CoV-2 nonstructural protein 1 (Nsp1) is the major pathogenesis factor that inhibits host translation using a dual strategy of impairing initiation and inducing endonucleolytic cleavage of cellular mRNAs. To investigate the mechanism of cleavage, we reconstituted it in vitro on β-globin, EMCV IRES, and CrPV IRES mRNAs that use unrelated initiation mechanisms. In all instances, cleavage required Nsp1 and only canonical translational components (40S subunits and initiation factors), arguing against involvement of a putative cellular RNA endonuclease. Requirements for initiation factors differed for these mRNAs, reflecting their requirements for ribosomal attachment. Cleavage of CrPV IRES mRNA was supported by a minimal set of components consisting of 40S subunits and eIF3g's RRM domain. The cleavage site was located in the coding region 18 nt downstream from the mRNA entrance, indicating that cleavage occurs on the solvent side of the 40S subunit. Mutational analysis identified a positively charged surface on Nsp1's N-terminal domain (NTD) and a surface above the mRNA-binding channel on eIF3g's RRM domain that contain residues essential for cleavage. These residues were required for cleavage on all three mRNAs, highlighting general roles of the Nsp1 NTD and eIF3g's RRM domain in cleavage per se, irrespective of the mode of ribosomal attachment.

[*Keywords*: SARS-CoV-2 Nsp1; eIF3g; mRNA cleavage; eukaryotic translation initiation; 40S ribosomal subunit]

Supplemental material is available for this article.

Received May 25, 2023; revised version accepted September 19, 2023.

Many viruses subvert cellular translation and mRNA surveillance/decay pathways to impair activation of innate immune pathways and to direct the translation apparatus to viral mRNAs (Abernathy and Glaunsinger 2015; Burgess et al. 2022). Host shutoff of translation and the resulting inhibition of type 1 interferon (IFN) induction and signaling are important aspects of the pathogenesis of members of the α-coronavirus (α-CoV) and β-coronavirus (β-CoV) genera of *Coronaviridae*, including the β-CoVs severe acute respiratory syndrome (SARS)-CoV and SARS-CoV-2 (Nakagawa and Makino 2021; Minkoff and TenOever 2023). Shutoff induced by coronaviruses involves endonucleolytic cleavage, leading to the degradation of cellular mRNAs as well as inhibition of splicing, nuclear export of mRNA, and cellular translation (Banerjee et al. 2020; Finkel et al. 2021; Nakagawa and Makino 2021; Zhang et al. 2021).

Although several coronavirus proteins have been implicated in the shutoff of translation (Banerjee et al. 2020; Thoms et al. 2020; Hsu et al. 2021), nonstructural protein 1 (Nsp1) is considered to be the major pathogenesis factor: It strongly dampens innate immune responses, and its mutation or partial deletion impairs replication of α-CoVs and β-CoVs in cells with an intact IFN response (Kamitani et al. 2006; Wathelet et al. 2007; Züst et al. 2007; Narayanan et al. 2008; Shen et al. 2019; Fisher et al. 2022). SARS-CoV and SARS-CoV-2 Nsp1s inhibit translation using a dual strategy of impairing the initiation process and inducing the endonucleolytic cleavage and subsequent degradation of cellular mRNAs (Kamitani et al. 2006; Narayanan et al. 2008; Huang et al. 2011; Finkel et al. 2012; Lokugamage et al. 2012; Mendez et al. 2021).

Nsp1 is cotranslationally cleaved from the N terminus of the ORF1a polyprotein (Snijder et al. 2003). SARS-CoV and SARS-CoV-2 Nsp1s are 180 amino acids long and conserved (84% identity), whereas α-CoV Nsp1s are more variable. SARS-CoV and SARS-CoV-2 Nsp1s have a structurally conserved ~120-amino-acid-long N-terminal

[1]**These authors contributed equally to this work.**
Corresponding author: tatyana.pestova@downstate.edu
Article published online ahead of print. Article and publication date are online at http://www.genesdev.org/cgi/doi/10.1101/gad.350829.123.

core that consists of an irregular seven-stranded β barrel, a long flanking α helix, and a short 3_{10} helix (Almeida et al. 2007; Clark et al. 2021; Semper et al. 2021; Wang et al. 2023). SARS-CoV-2 Nsp1 contains an additional 3_{10} helix and β strand. The C-terminal region (amino acids 126–180) of SARS-CoV-2 Nsp1 is unstructured (Wang et al. 2023), but when bound to the 40S ribosomal subunit, amino acids 154–180 form two short α helices (Schubert et al. 2020; Thoms et al. 2020; Yuan et al. 2020). On the 40S subunit, the C-terminal α-helical minidomain is inserted into the entrance portion of the mRNA-binding channel, where it interferes with binding of mRNA (Schubert et al. 2020; Thoms et al. 2020; Yuan et al. 2020). The exact ribosomal position of the Nsp1 NTD that is flexibly connected to the C-terminal minidomain is obscure, even though it has been shown that it cross-links to the eIF3g subunit of eIF3 and some ribosomal proteins that reside at the mRNA entrance (Graziadei et al. 2022).

The ribosomal position of the C-terminal α-helical minidomain accounts for the mechanism for inhibition of protein synthesis by SARS-CoV and SARS-CoV-2 Nsp1s by steric clashing of this domain with mRNA. In contrast, the mechanism by which Nsp1 induces endonucleolytic cleavage of cellular mRNAs that is followed by their Xrn1-mediated degradation (Kamitani et al. 2009; Huang et al. 2011; Gaglia et al. 2012; Mendez et al. 2021; Fisher et al. 2022) remains unknown. SARS-CoV Nsp1 alone does not mediate cleavage of mRNAs, and this process depends on the presence of 40S subunits and is restricted to translationally active mRNAs (Kamitani et al. 2009; Gaglia et al. 2012). Cleavage sites map to the 5′ UTR and proximal coding region of capped mRNAs and to the vicinity of the initiation codon at the 3′ border of poliovirus and encephalomyocarditis (EMCV) virus IRESs (Kamitani et al. 2009; Huang et al. 2011; Tardivat et al. 2023). Hepatitis C virus (HCV) and cricket paralysis virus (CrPV) IRESs did not undergo SARS-CoV Nsp1-induced cleavage in cell-free extracts (Kamitani et al. 2009). The positions of cleavages and their dependence on the mechanism of translation initiation led to the suggestion that cleavage occurs at the stage of ribosomal attachment before establishment of codon–anticodon interaction (Nakagawa and Makino 2021). Nsp1-induced cleavage required its ribosomal association, and consistently, cleavage was inhibited by K164A/H165A substitutions in SARS-CoV and SARS-CoV-2 Nsp1s that abrogate their ribosomal binding (Lokugamage et al. 2012; Tardivat et al. 2023). Importantly, R125A/K126A substitutions at the C-terminal border of the NTD of SARS-CoV Nsp1 (Lokugamage et al. 2012) and analogous substitutions in SARS-CoV-2 Nsp1 (Mendez et al. 2021) abrogated Nsp1-induced mRNA cleavage but did not affect its ability to inhibit translation, separating the RNA cleavage and the translation inhibition functions of Nsp1. Nsp1's lack of independent cleavage activity and of sequence or structural homology with ribonucleases (Almeida et al. 2007) led to the suggestion that it recruits a specific cellular endonuclease to a subset of ribosomal initiation complexes (Kamitani et al. 2009; Nakagawa and Makino 2021).

Here, we investigated the mechanism of Nsp1-induced cleavage by reconstituting this process in vitro from individual purified translation components on three mRNAs that use unrelated translation initiation mechanisms.

Results

In vitro reconstitution reveals that canonical translation initiation components are sufficient for SARS-CoV-2 Nsp1 to induce cleavage of 5′ end-dependent mRNAs

To confirm the ability of recombinant, bacterially expressed SARS-CoV-2 Nsp1 to inhibit initiation on 5′ end-dependent mRNA, we assayed its influence on 48S complex formation on $(CAA)_4$-MF β-globin mRNA comprising four 5′-terminal CAA repeats that allow efficient cap-independent initiation (Pestova and Kolupaeva 2002) followed by the β-globin 5′ UTR, a short (MF) open reading frame, a stop codon, and a 110-nt-long 3′ UTR (Fig. 1A). 48S complexes were reconstituted in vitro from individual translation components (40S subunits, initiation factors, and Met-$tRNA_i^{Met}$) in the absence or presence of Nsp1. Toeprinting involves extension by reverse transcriptase (RT) of a primer annealed to the ribosome-bound mRNA: cDNA synthesis is arrested by the leading edge of the 40S subunit, yielding toeprints +15–17 nt downstream from the P-site codon. Strikingly, preincubation of 40S subunits with Nsp1 not only inhibited 48S complex formation but also yielded prominent bands at discrete positions in the 5′ UTR (Fig. 1B, lanes 2,3). Persistence of these bands when reverse transcription was done after phenol extraction (Fig. 1B, lanes 12,13) indicated that they corresponded to sites of mRNA cleavage rather than to specific binding of translation components. The most 5′-terminal cleavage occurred 11–12 nt from the 5′ end, and downstream cleavages were all separated by ~6–8 nt (summarized in Fig. 1A). eIF2 was not required for cleavage (Fig. 1B, lane 7), whereas 40S subunits, eIF3, and group 4 eIFs (eIF4A/$eIF4G_{736–1115}$/eIF4B) were essential (Fig. 1C). Omission of eIF4B moderately reduced cleavage (Fig. 1B, lane 5) but had a stronger effect when the concentration of eIF4G was reduced (Fig. 1D, lanes 5,6). Cleavage was not influenced by eIF1 and eIF1A (Fig. 1D, lanes 7–9).

To monitor mRNA cleavage directly, we used 5′- and 3′-labeled $(CAA)_4$-MF β-globin mRNAs. For 5′ labeling, mRNA was capped using [α-^{32}P]GTP, whereas 3′ labeling was done by ligation of mRNA with 5′[^{32}P]pCp. Factor requirements and the positions of cleavages on 3′-labeled mRNA (Supplemental Fig. S1A) were identical to those observed using the reverse transcription technique (Fig. 1B–D). Cleavage of 5′-labeled mRNA also showed the same factor requirements but yielded only one labeled product corresponding to the 5′-terminal cleavage site (Fig. 1E). The time course of Nsp1-induced cleavage monitored by reverse transcription revealed progressive accumulation of shorter mRNA products (Fig. 1F). However, cleavage of 5′-labeled mRNA in conditions of the longest incubation time still yielded only the 5′-terminal cleavage product (Supplemental Fig. S1B). These results indicate that cleavage is sequential and starts from the 5′-terminal site.

To assay the influence of Nsp1 on mRNA in 80S ribosomal complexes and their ability to elongate, we used

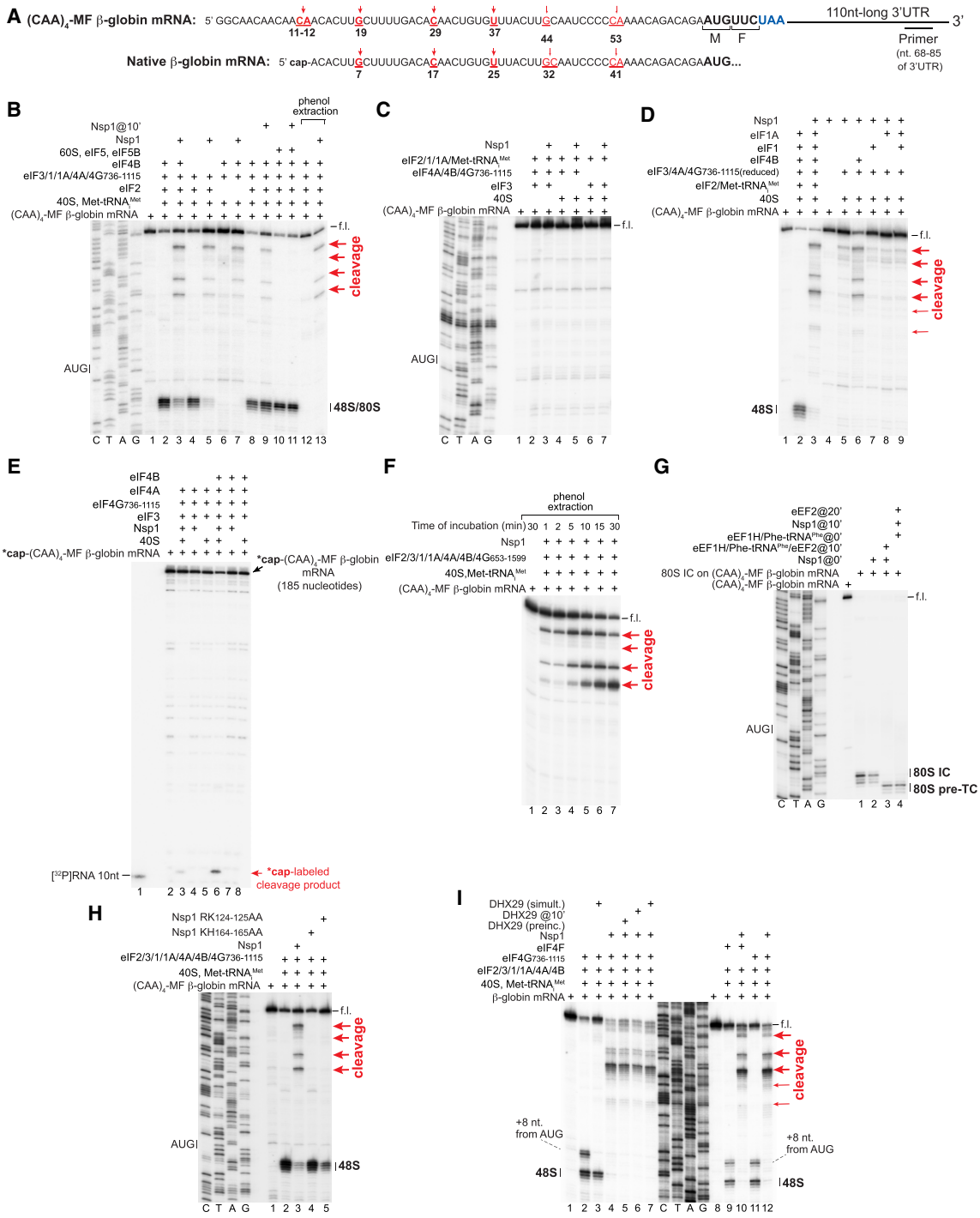

Figure 1. SARS-CoV-2 Nsp1-induced cleavage of mRNA during 5′ end-dependent initiation. (*A*) Schematic representation of $(CAA)_4$-MF β-globin and native β-globin mRNAs, annotated to show the 5′ UTR, coding region, stop codon, sites of Nsp1-mediated cleavage (red arrows), and the position of the toeprinting primer. (*B–D*) The influence of wt Nsp1 on 48S complex formation on $(CAA)_4$-MF mRNA and on its integrity in the presence of the indicated translation components, assayed by toeprinting or, where indicated, by primer extension by RT after phenol extraction of mRNA. (*E*) Nsp1-induced cleavage of 5′[^{32}P]cap-labeled $(CAA)_4$-MF mRNA depending on the presence of the indicated translation components, assayed directly after phenol extraction. A 10-nt-long 5′[^{32}P]-labeled oligo RNA was used as a marker. (*F*) Time course of Nsp1-induced cleavage of $(CAA)_4$-MF β-globin in the presence of the indicated translation components, assayed by primer extension by RT after phenol extraction of mRNA. (*G*) The influence of wt Nsp1 on $(CAA)_4$-MF β-globin mRNA in preassembled 80S initiation complexes and their ability to undergo elongation, assayed by toeprinting. (*H*) The influence of wt and $RK_{124–125}AA$ or $KH_{164–165}AA$ mutant Nsp1 on 48S complex formation on $(CAA)_4$-MF β-globin mRNA and on its integrity in the presence of translation components as indicated, assayed by toeprinting. (*I*) The influence of wt Nsp1 on 48S complex formation on native β-globin mRNA and on its integrity in the presence of the indicated translation components, assayed by toeprinting.

80S initiation complexes obtained by incubation of reconstituted 48S complexes with eIF5, eIF5B, and 60S subunits. Incubation of such 80S complexes with Nsp1 did not induce mRNA cleavage (Fig. 1B, lane 11) or affect their ability to undergo elongation upon addition of elongation factors and cognate elongator tRNA (Fig. 1G).

The $KH_{164–165}AA$ Nsp1 mutant, which lacks the ability to bind to the 40S subunit (Schubert et al. 2020; Thoms et al. 2020), did not influence 48S complex formation or induce cleavage of $(CAA)_4$-MF β-globin mRNA (Fig. 1H, lane 4), whereas the $RK_{124–125}AA$ Nsp1 mutant, which inhibits translation but lacks mRNA cleavage activity in vivo (Lapointe et al. 2021; Mendez et al. 2021), also did not induce cleavage but retained the ability to inhibit 48S complex formation in our in vitro reconstituted system (Fig. 1H, lane 5). Thus, the activities of Nsp1 mutants in the reconstituted system were consistent with their reported activities in vivo.

To determine whether the eIF4E–cap interaction influences cleavage, we compared the effect of Nsp1 on native capped β-globin mRNA in the presence of native eIF4F or the $eIF4G_{736–1115}$ middle domain. In the presence of eIF4F, we again observed several discrete cleavage sites, with the first site slightly closer to the 5′ end than in the case of the $(CAA)_4$-MF β-globin mRNA but with a similar spacing between them (Fig. 1I, lane 10). The positions of cleavage sites coincided with those (starting from the second site) that were observed in the case of $(CAA)_4$-MF β-globin mRNA (summarized in Fig. 1A). The second and third cleavage sites coincided with those observed by the reverse transcription technique in rabbit reticulocyte lysate (RRL) supplemented with SARS-CoV Nsp1 (Huang et al. 2011), whereas the first cleavage site coincided with that of cap-labeled β-globin mRNA in RRL supplemented with SARS-CoV-2 Nsp1 (Tardivat et al. 2023). Cleavage sites were identical in the presence of eIF4F and $eIF4G_{736–1115}$ (Fig. 1I, lanes 10,12). As expected, addition of DHX29 that resides at the mRNA entrance (Hashem et al. 2013a) eliminated the aberrant toeprint +8 nt from the AUG codon corresponding to incompletely closed 48S complexes (Fig. 1I, lanes 2,3; Abaeva et al. 2011) but did not affect cleavage irrespective of the time of DHX29 addition (Fig. 1I, lanes 4–7). Thus, Nsp1-induced cleavage was not affected by the eIF4E–cap interaction or by DHX29.

The positions of Nsp1-induced cleavage sites at the beginning of the 5′ UTR, the dependence of cleavage on 40S subunits and group 4 eIFs but not on eIF2, and the fact that cleavage is reduced by delayed addition of Nsp1 to preformed 48S complexes are consistent with the suggestion that the process occurs at the stage of ribosomal attachment before establishment of the codon–anticodon interaction (Nakagawa and Makino 2021). However, our in vitro reconstitution results argue against involvement in the process of a putative cellular RNA endonuclease.

SARS-CoV-2 Nsp1-induced cleavage of EMCV IRES mRNA

Next, we assayed Nsp1's influence on mRNAs translated by internal ribosomal entry rather than by 5′ end-dependent initiation. The ~450-nt-long EMCV internal ribosomal entry site (IRES) comprises five domains: H–L (Fig. 2A). The Yn-Xm-AUG motif located at the 3′ border of the IRES (Yn indicates pyrimidine tract, and Xm indicates spacer) contains AUG_{834}, the native initiation codon. Initiation on viral IRESs relies on their specific interactions with canonical components of the translation apparatus. The only such interaction identified so far for the EMCV IRES is that of its JK domain with the central domain of eIF4G (Pestova et al. 1996), which is enhanced by eIF4A (Lomakin et al. 2000). After binding to the JK domain, eIF4G/eIF4A restructure the 3′ border of the IRES (Kolupaeva et al. 2003), likely facilitating attachment of 43S complexes. However, the JK domain is not sufficient for IRES activity, which also requires the upstream domain I, whose function is unknown.

In vitro reconstitution on the EMCV IRES mRNA yielded 48S complexes predominantly assembled on AUG_{834}, although low-level 48S complex formation also occurred at AUG_{826} and AUG_{846} (Fig. 2B, lane 3). Preincubation of 40S subunits with Nsp1 resulted in the appearance of additional bands (Fig. 2B, lane 4), and reverse transcription done after phenol extraction confirmed that they correspond to four discrete cleavage sites ~6–9 nt apart and with the 5′-terminal site 2–3 nt upstream of AUG_{834} (Fig. 2B [lane 10], summarized in A). Cleavage sites coincided with those observed when SARS-CoV Nsp1 was added to the reconstituted system (Fig. 2C) and to RRL (Huang et al. 2011). Again, cleavage was 40S-dependent and was reduced by delayed addition of Nsp1 (Fig. 2B, lanes 11,12).

Consistent with the essential role of eIF4G in ribosomal attachment to the EMCV IRES (Pestova et al. 1996), cleavage was abolished by omission of eIF4G (Fig. 2D, lane 4). However, in contrast to 5′ end-dependent mRNAs, cleavage was also strongly reduced in the absence of eIF2 • GTP/Met-$tRNA_i^{Met}$ (Fig. 2D, lane 3). Mutations in the IRES that influenced 48S complex formation (e.g., disruption of the apex of domain I) (Fig. 2A), also strongly reduced cleavage (Fig. 2D, lane 5). As in the case of 5′ end-dependent mRNAs, cleavage was not affected by DHX29 (Fig. 2E), and the $RK_{124–125}AA$ Nsp1 mutant did not induce cleavage but retained the ability to inhibit 48S complex formation (Fig. 2F). The factor requirements and positions of cleavage sites observed by direct monitoring of 3′-labeled EMCV IRES mRNA (Supplemental Fig. S1C) were identical to those observed using the reverse transcription technique.

In contrast to $(CAA)_4$-MF β-globin mRNA, the time course of Nsp1-induced cleavage of EMCV IRES mRNA did not show accumulation of the shortest mRNA product, and the relative intensities of cleavages at the strongest first and third positions remained the same (Supplemental Fig. S2A). We were unable to use 5′-labeled EMCV IRES mRNA to identify the primary cleavage sites because 5′-terminal cleavage products (~460 nt) are too large to be sufficiently resolved on a sequencing gel and therefore introduced mutations downstream from the JK domain (Supplemental Fig. S2B) and tested their influence on Nsp1-mediated cleavage. Deletion of domain L did not

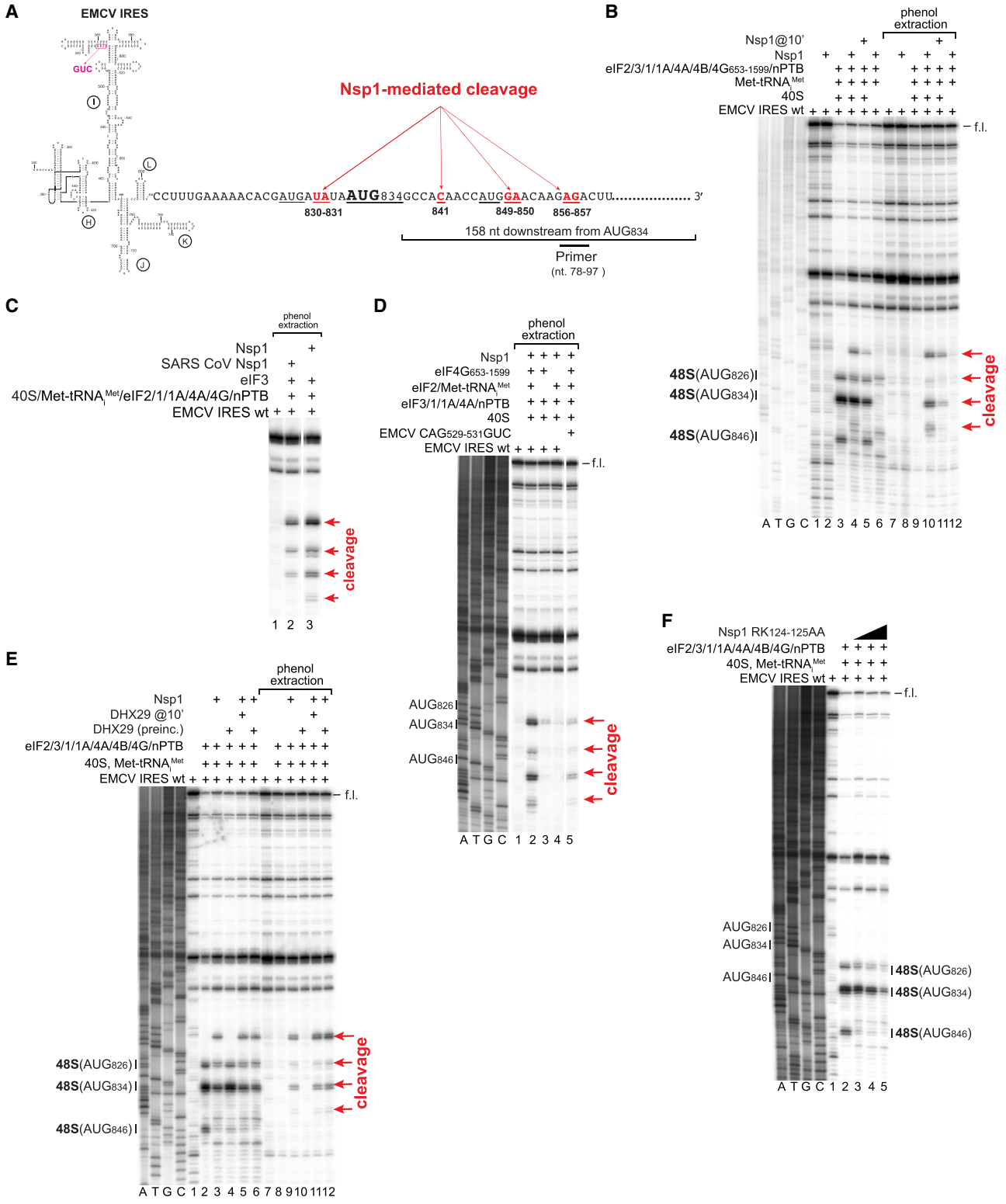

Figure 2. SARS-CoV-2 Nsp1-induced cleavage of mRNA during EMCV IRES-mediated initiation. (*A*) Schematic representation of the EMCV IRES and the proximal coding region, annotated to show IRES domains, the inactivating $CAG_{529–531}GUC$ substitutions, the initiation codon, the position of the toeprinting primer, and sites of Nsp1-induced cleavage (red arrows). (*B–F*) The influence of wt SARS-CoV-2 Nsp1 (*B*), wt SARS-CoV-2 and wt SARS-CoV Nsp1s (*C*), wt SARS-CoV-2 Nsp1 (*D*,*E*), and $RK_{124–125}AA$ SARS-CoV-2 Nsp1 mutant (*F*) on 48S complex formation on wt (*B*,*C*,*E*,*F*) and $CAG_{529–531}GUC$ mutant (*D*) EMCV IRES mRNAs as well as on mRNA integrity in the presence of the indicated translation components, assayed by toeprinting or, where indicated, by primer extension by RT after phenol extraction of mRNA. Separation of lanes in *C* and *D* by white lines indicates that these parts were juxtaposed from the same gel.

influence cleavage, whereas its replacement by 4 or 8 nt slightly reduced its efficiency at the last two sites (Supplemental Fig. S2C). Stabilization and particularly destabilization of domain L moderately inhibited cleavage at all sites (Supplemental Fig. S2D, lanes 2,4,6). Strikingly, introduction of three substitutions in the region surrounding the 5′-terminal site specifically abolished cleavage at the first two positions (Supplemental Fig. S2D, lanes 2,8). These mutations included replacement of AUG_{826} and AUG_{834} by AUC codons. To determine whether the presence of the immediate upstream AUG codon is required for cleavages, we determined how replacing AUG_{846} with AUC and substituting the downstream AAG_{853} with AUG would influence the efficiency and the positions of the two downstream cleavage sites. These changes did not influence cleavage at the two downstream sites (Supplemental Fig. S2E), arguing against the requirement of the immediate upstream AUG codon for Nsp1-induced cleavage. These data indicate that cleavage at the first and second pairs of sites occur independently and suggest the possibility of some nucleotide specificity of Nsp1-induced cleavage.

In conclusion, Nsp1-induced cleavage of the EMCV IRES mRNA also required only canonical translation components and occurred at the stage of ribosomal attachment.

Reconstitution of Nsp1-induced cleavage of cricket paralysis virus (CrPV) IRES mRNA reveals the minimal set of translation components that can support cleavage

Ribosomal attachment to 5′ end-dependent and EMCV IRES-containing mRNAs relies on large, strongly overlapping sets of initiation factors. To investigate whether Nsp1-mediated cleavage can be achieved with a smaller set of eIFs, we took advantage of factor-independent ribosomal attachment to the CrPV IGR IRES. This IRES comprises three pseudoknots (PKI–PKIII) (Fig. 3A). Stem–loops SL2.1 and SL2.3 in PKIII contain conserved apical motifs that interact with ribosomal proteins on the head of the 40S subunit (Muhs et al. 2011; Fernández et al. 2014), whereas PKI mimics the anticodon stem–loop of tRNA base-paired to a cognate codon (Costantino et al. 2008). The IRES binds directly to 40S subunits or to 80S ribosomes (Wilson et al. 2000; Pestova et al. 2004). In the resulting complexes, the IRES is located in the intersubunit space, with PKI mimicking the tRNA/mRNA interaction in the decoding center of the ribosomal A site (Fernández et al. 2014).

Although the CrPV IRES was shown to be able to bind to 40S subunits simultaneously with Nsp1 (Yuan et al. 2020), Nsp1 affected ribosomal interaction and positioning of the IRES (Lokugamage et al. 2012; Yuan et al. 2020). Consistent with the previous report (Lokugamage et al. 2012), preincubation of 40S subunits with Nsp1 did not induce cleavage of CrPV mRNA; however, in contrast to both reports (Lokugamage et al. 2012; Yuan et al. 2020), it also did not affect the 40S/CrPV IRES interaction and accommodation of mRNA in the mRNA-binding channel, yielding the same intensity toeprints corresponding to 40S/IRES and 80S/IRES complexes (Fig. 3B). The reason for the observed discrepancy could result from differences in the coding regions. In our study, the IRES was followed by a long native viral coding region, whereas in the previous studies, the coding region was either native but short (Yuan et al. 2020) or had been replaced by a heterologous reporter (Lokugamage et al. 2012). Although it was possible that binding of the IRES to 40S/Nsp1 complexes displaced Nsp1 from the 40S subunit in our experiments, another study had previously shown that after binding of 40S/Nsp1 complexes to CrPV IRES mRNA containing a 48-nt-long coding region, Nsp1 remained long associated with the 40S subunit complex (Lapointe et al. 2021). This prompted us to investigate the ability of different eIFs to support Nsp1-induced cleavage of CrPV IRES mRNA.

Although the CrPV IRES and eIF2/Met-$tRNA_i^{Met}$ would clash on the 40S subunit, the simultaneous presence of the IRES and eIF3 is allowed (Pestova et al. 2004). Strikingly, inclusion of eIF3 in reaction mixtures resulted in strong Nsp1-induced cleavage at nucleotides 6246–6247 (18 nt downstream from the toeprint corresponding to the 40S/IRES complex) and an additional low-intensity cleavage at nucleotide 6256 (Fig. 3C, lanes 5,12). Additional inclusion of eIF4A/eIF4G resulted in three prominent discrete downstream cleavages, again ~6–9 nt apart (Fig. 3C [lanes 4,11], summarized in 3A). Further supplementation of reaction mixtures with eIF2, eIF1, eIF1A, and Met-$tRNA_i^{Met}$ enhanced accumulation of short mRNA products (Fig. 3C, lanes 6,13). eIF4A/eIF4G could potentially stimulate cleavage at the first 5′-terminal site and promote downstream cleavage without prior dissociation of truncated mRNA products. Alternatively, downstream cleavage of truncated mRNA products could result from their de novo 5′ end-dependent attachment to 40S subunits associated with various sets of eIFs, like in the case of $(CAA)_4$-MF β-globin mRNA. The previously reported lack of cleavage of CrPV IRES mRNA in RRL upon addition of SARS-CoV Nsp1 (Kamitani et al. 2009) could be due to initiation occurring by direct binding of the IRES to 80S ribosomes rather than to 40S subunits because of their engagement into 43S complexes (Pestova et al. 2004).

Next, we determined whether eIF3 can be replaced by any of its subunits, focusing on the eIF3b-g-i module that, like Nsp1, resides at the mRNA entrance (des Georges et al. 2015). Individual recombinant eIF3g could substitute for native eIF3 in supporting Nsp1-induced cleavage (Fig. 3D, lanes 6,7). However, in contrast to native eIF3, inclusion of eIF4A/eIF4G in reaction mixtures containing eIF3g did not stimulate downstream cleavages (Fig. 3D, lanes 9,10), which is consistent with the lack of interaction between eIF3g and eIF4G and therefore the lack of coupling of eIF4A/eIF4G helicase activity with ribosomal complexes. Importantly, cleavage was IRES-dependent, and mutations in the 40S-interacting SL2.3 loop and destabilizing mutations in PKIII (Fig. 3A), which strongly impair 40S/IRES complex formation (Costantino and Kieft 2005), also impaired Nsp1-induced cleavage (Fig. 3E, lanes 6–15). eIF3g was not able to replace native eIF3 in supporting Nsp1-induced cleavage on EMCV IRES

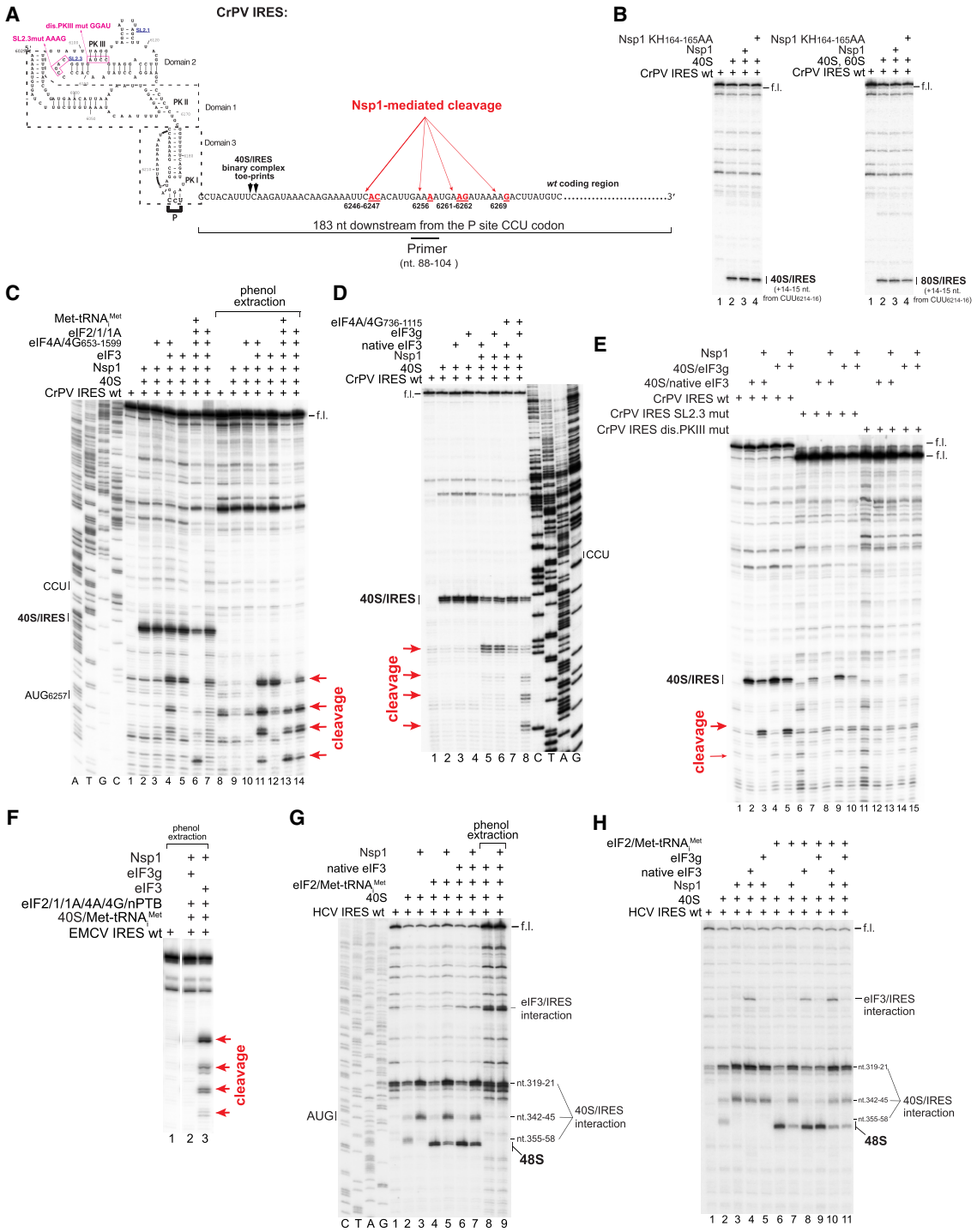

Figure 3. SARS-CoV-2 Nsp1-induced cleavage of mRNA during CrPV and HCV IRES-mediated initiation. (*A*) Schematic representation of the CrPV IRES with the proximal cognate coding region, annotated to show IRES domains, pseudoknots, stem–loops SL2.1 and SL2.3, inactivating substitutions in domain 2, the P-site codon, the position of 40S/IRES toeprints, the position of the toeprinting primer, and sites of Nsp1-mediated cleavage (red arrows). (*B*) The influence of wt and $KH_{164–165}AA$ Nsp1 on association of CrPV IRES mRNA with 40S subunits and 80S ribosomes assayed by toeprinting. (*C–E*) Cleavage of wt (*C*,*D*) or inactivated SL2.3 and PKIII mutant (*E*) CrPV IRES mRNAs depending on the presence of wt Nsp1 and various translation components, assayed by toeprinting or, where indicated, by primer extension by RT after phenol extraction of mRNA. (*F*) Cleavage of wt EMCV IRES mRNA depending on the presence of wt Nsp1 and translation components as indicated, assayed by primer extension after phenol extraction of mRNA. (*G*,*H*) The influence of wt Nsp1 on ribosomal binding and the integrity of the HCV IRES depending on the presence of various translation initiation components, assayed by toeprinting or, where indicated, by primer extension after phenol extraction of mRNA. Separation of lanes in *F* by a white line indicates that these parts were juxtaposed from the same gel.

mRNA, highlighting the requirement for native eIF3 for ribosomal attachment to this IRES (Fig. 3F).

Visualization of cleavage using 3′-labeled CrPV IRES mRNA did not reveal any differences in the positions of cleavage from those determined by the reverse transcription technique (Supplemental Fig. S1D). In the case of 5′-labeled CrPV IRES mRNA, only one identical 5′-terminal fragment was observed in the presence of eIF3g or eIF3 in combination with eIF4G/4A (Supplemental Fig. S1E, lanes 3,8), confirming that in both cases cleavage starts from the same 5′-terminal site, whereas downstream cleavages occur sequentially on 3′-terminal fragments.

We next investigated the influence of Nsp1 on the HCV IRES. As in the case of the CrPV IRES, ribosomal recruitment to the HCV IRES occurs by its direct binding to the 40S subunit, although further initiation events differ drastically and initiation requires eIF2/Met-tRNA$_i^{Met}$ (Pestova et al. 1998). Association of the HCV IRES with the 40S subunit also displaces eIF3, usurping its ribosomal contacts (Hashem et al. 2013b). In 40S/IRES binary complexes, Nsp1 eliminated toeprints at nucleotides 355–358, which signal correct accommodation of mRNA in the mRNA-binding channel, but did not affect toeprints at nucleotides 319–321 and 342–345, which correspond to upstream 40S/IRES contacts (Fig. 3G,H, lanes 1–3; Pestova et al. 1998). It also strongly reduced toeprints corresponding to 48S complexes (Fig. 3G [lanes 4,5], H [lanes 6,7]). Addition of eIF3 did not stimulate cleavage (Fig. 3G [lanes 6–9], H [lanes 4,10]). Although this could be explained by IRES-mediated displacement of eIF3 from the 40S subunit, individual eIF3g also did not support cleavage (Fig. 3H, lanes 5,11). Thus, in contrast to the CrPV IRES, in Nsp1-containing ribosomal complexes, the coding region of the HCV IRES mRNA is not accommodated in the mRNA-binding channel and therefore does not reach the nuclease active center.

In conclusion, reconstitution of Nsp1-induced cleavage of the CrPV IRES mRNA revealed that it requires the minimal set of translation components, which consists of a 40S subunit and eIF3g.

Mutational analysis of eIF3g

The 320-amino-acid-long eIF3g comprises the N-terminal region, which is involved in formation of the eIF3b-g-i module (Asano et al. 1998; Herrmannová et al. 2012), and the C-terminal RRM domain (amino acids 232–320) (Cuchalová et al. 2010; Brito Querido et al. 2020). The eIF3b-g-i module interacts with the 40S subunit through the contacts of the β-propeller domain of eIF3b with the ribosomal protein uS4, whereas the C-terminal RRM domain of eIF3g was recently assigned to cryo-EM density at the mRNA entry and, accordingly, interacts with helix (h) 16 of 18S rRNA and ribosomal proteins uS3 and eS10 (des Georges et al. 2015; Brito Querido et al. 2020). To determine the region of eIF3g required for Nsp1-mediated mRNA cleavage, we expressed a series of deletion mutants guided by its secondary and tertiary structure elements (Fig. 4A). The small eIF3g RRM domain comprising only 89 amino acids was necessary and sufficient for Nsp1-induced cleavage of the CrPV IRES mRNA (Fig. 4B).

The canonical RRM domain adopts a β1α1β2β3α2β4 fold with an antiparallel four-stranded β sheet packed against two perpendicular α helices. The β sheet contains two RNP motifs located in β1 and β3 strands. To examine the functional importance of specific regions of eIF3g in supporting Nsp1-induced mRNA cleavage, we generated eIF3g mutants with Ala substitutions of individual charged surface-exposed residues in the RRM domain guided by the model of the 48S complex (Brito Querido et al. 2020), including residues in both RNP motifs and in the conserved positively charged loop between β2 and β3 strands, which was modeled to interact with h16 (Fig. 4C). The activities of all tested mutants are shown in Figure 4, D and E: Mutants that lost or had severely reduced activity are in red, whereas mutants with moderately reduced activity are in orange. Substitution of key residues in RNP1 position 1 (K280A) and RNP2 position 2 (R242A) abrogated Nsp1-induced cleavage of the CrPV IRES mRNA (Fig. 4D, lanes 4,9). Notably, a basic amino acid occurs at RNP2 position 2 in all eIF3g RRM domains (Fig. 4C), whereas the canonical RNP2 motif contains an aromatic residue in this position (Muto and Yokoyama 2012). Substitution of K274 in the loop between β2 and β3 and of the neighboring K272 and D273 also abrogated mRNA cleavage (Fig. 4D [lanes 7,8], E [lane 5]). An equally strong inactivating effect was observed after R267A substitution in the β2 strand (Fig. 4E, lane 4). A basic amino acid at this position is a conserved feature of eIF3g (Fig. 4C). Substitution of the neighboring H288, R289, and R290 caused only a minor impairment of the efficiency of cleavage (Fig. 4D [lane 10], E [lanes 6,7]). Interestingly, cleavage was slightly elevated in the presence of eIF3g with the E257A substitution in helix α1 (Fig. 4D, lane 5).

Mutations in the eIF3g RRM domain that impaired Nsp1-induced mRNA cleavage included critical residues in its RNP motifs and were located on the surface above the mRNA-binding channel (Fig. 4F).

To determine whether eIF3g is equally important for Nsp1-induced cleavage of 5′ end-dependent and EMCV IRES-containing mRNAs, which require complete eIF3 for ribosomal attachment, we used native eIF3 containing either wt or mutated eIF3g. For this, Expi293 cells were transfected with expression vectors for FLAG-tagged wt, R242A, or R267A eIF3g. Wt and mutated FLAG-tagged eIF3g efficiently incorporated into eIF3, which contained the canonical set of other subunits (Fig. 5A). eIF3s containing wt, R242A, or R267A FLAG-tagged eIF3g were equally active in supporting 48S complex formation on $(CAA)_4$-MF β-globin mRNA (Fig. 5B, lanes 2,4,6) and on EMCV IRES mRNA (Fig. 5C, lanes 2,4,6). In all cases, Nsp1 inhibited 48S complex formation (Fig. 5B,C, lanes 3,5,7). However, eIF3 containing R242A mutant eIF3g was substantially less active than eIF3 containing wt eIF3g in supporting Nsp1-induced cleavage on all three mRNAs: EMCV IRES-containing, CrPV IRES-containing, and $(CAA)_4$-MF β-globin mRNAs (Fig. 5D). The activity of eIF3 containing eIF3g(R267A) was even lower than that of eIF3 containing eIF3g(R242A) in supporting Nsp1-induced cleavage (Fig. 5E).

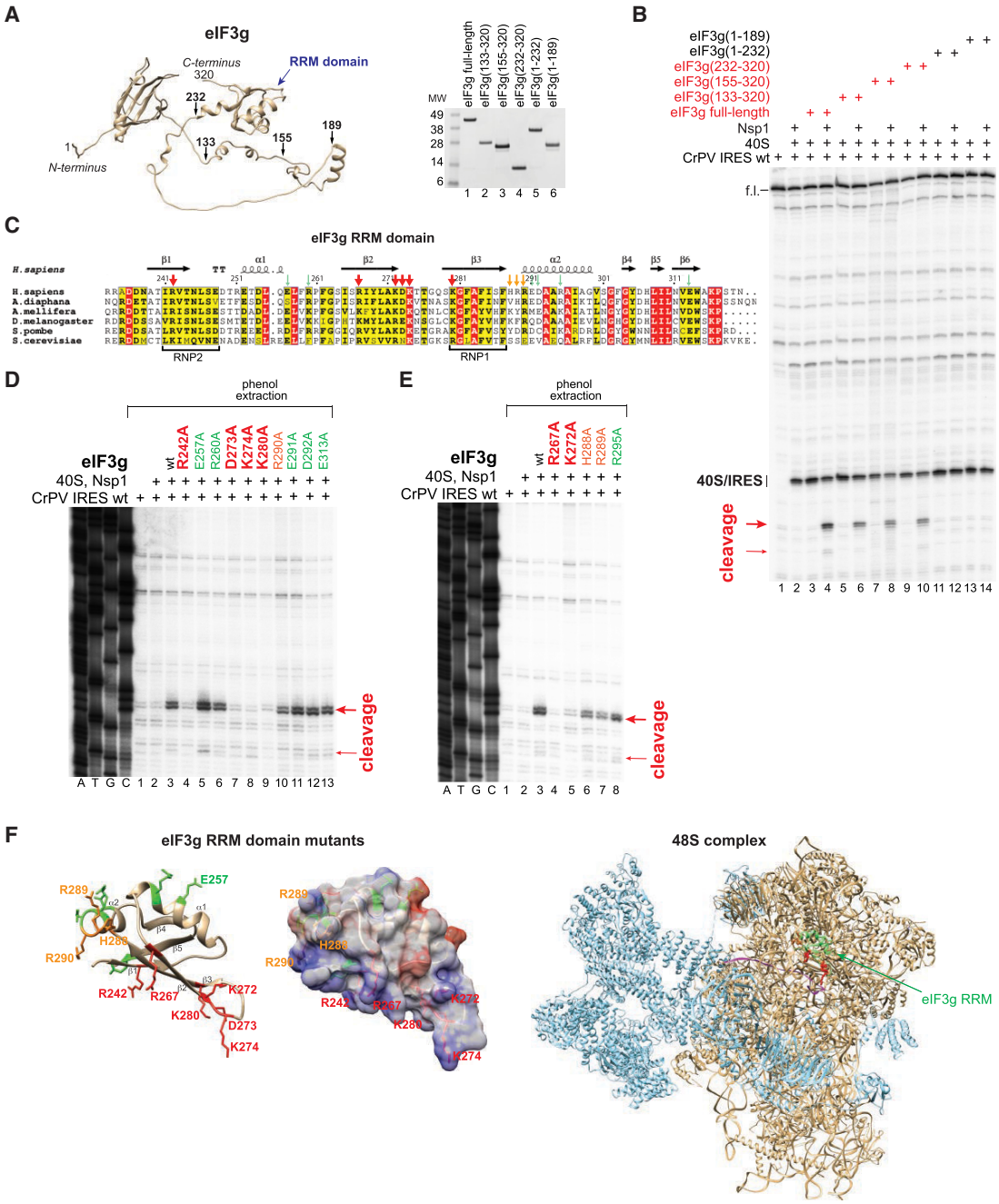

Figure 4. Determination of eIF3g regions required for Nsp1-induced cleavage of CrPV IRES mRNA. (*A*, *left* panel) Model of the AlphaFold structure of human eIF3g labeled to show the RRM domain and amino acid residues at the borders of eIF3g truncation mutants (black arrows). (*Right* panel) Purified eIF3g truncation mutants, assayed by SDS-PAGE followed by SimplyBlue staining. (*B*) The activities of eIF3g mutants in supporting Nsp1-induced cleavage of wt CrPV IRES mRNA, assayed by toeprinting. (*C*) Amino acid sequence alignment of the RRM domain of human eIF3g with that of other species, done using Clustal Omega. Residues boxed in red are identical. Secondary structure elements from the structure of the human eIF3g RRM domain (PDB: 2CQ0) are represented schematically *above* the sequence alignment, and the RNP1 and RNP2 motifs are indicated *below* the sequence alignment. The amino acid sequence of *Homo sapiens* eIF3g (NP_003746.2) between residues 233 and 320 is aligned with its *Exaiptasia diaphana* (XP_020896357), *Drosophila melanogaster* (NP_650887), *Apis mellifera* (XP_391934), *Schizosaccharomyces pombe* (NP_595727), and *Saccharomyces cerevisiae* (NP_010717) homologs. Residues substituted by Ala are indicated by arrows, inactivating mutations are in red, mutations causing a minor reduction in the efficiency of cleavage are in orange, and mutations that had no effect on cleavage are in green (summary of results is presented in *D* and *E*). (*D*,*E*) The activities of eIF3g RRM domain mutants in supporting Nsp1-induced cleavage of wt CrPV IRES mRNA, assayed by primer extension after phenol extraction of mRNA. Inactivating mutations are in red, mutations causing a minor reduction in the efficiency of cleavage are in orange, and mutations that do not affect cleavage are in green. (*F*) Ribbon diagram (*left* panel) and surface charge distribution (*middle* panel) of the eIF3g RRM domain (PDB: 6ZMW), annotated to show mutated residues (sticks) colored according to their activity (shown in *D*,*E*). (*Right* panel) The 48S initiation complex model (PDB: 6ZMW) showing the RRM domain of eIF3g (green ribbon) with amino acids that are essential for Nsp1-induced mRNA cleavage (red and orange sticks); other subunits of eIF3 (light-blue ribbon); 40S ribosomal subunit, other initiation factors, and Met-tRNA$_i^{Met}$ (tan ribbons); and mRNA (magenta ribbon).

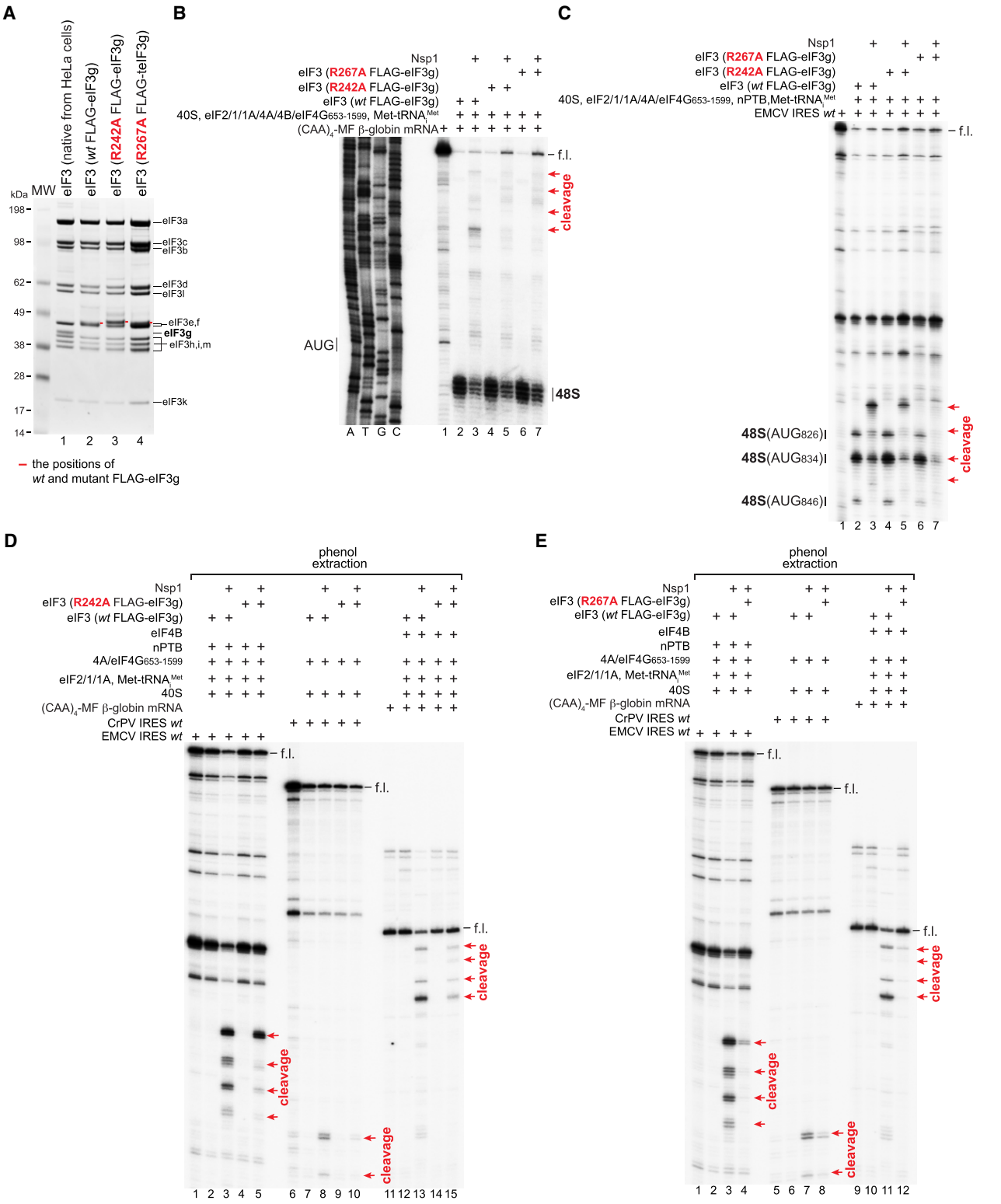

Figure 5. The importance of eIF3g for Nsp1-induced cleavage of β-globin and EMCV IRES-containing mRNAs. (*A*) Purified native eIF3 from HeLa cells and eIF3 containing FLAG-tagged wt or mutant eIF3g expressed in Expi293 cells, analyzed by SDS-PAGE followed by SimplyBlue staining. (*B*,*C*) The activity of eIF3 containing FLAG-tagged wt or mutant eIF3g in 48S complex formation on $(CAA)_4$-MF β-globin (*B*) and EMCV IRES (*C*) mRNAs in the presence of the indicated translation components with/without wt Nsp1, assayed by toeprinting. (*D*,*E*) The activities of eIF3 containing either wt or mutant FLAG-tagged eIF3g in supporting Nsp1-induced cleavage of $(CAA)_4$-MF β-globin, CrPV IRES, and EMCV IRES mRNAs in the presence of the indicated translation components, assayed by primer extension after phenol extraction of mRNA.

In conclusion, full-length eIF3g could be substituted by its C-terminal RRM domain during Nsp1-induced cleavage of the CrPV IRES mRNA. Importantly, this domain had an essential role in Nsp1-induced cleavage on all tested mRNAs, irrespective of the modes of their ribosomal attachment.

Mutational analysis of Nsp1

Mutagenesis of the Nsp1 NTD and the linker region was guided by surface exposure, charge (Clark et al. 2021; Semper et al. 2021), and conservation (Supplemental Fig. S3). The activities of Nsp1 Ala substitution mutants in inducing mRNA cleavage were essentially the same on different mRNAs irrespective of their mode of initiation. The activities of all mutants are shown for the EMCV IRES mRNA in Figure 6, A–C. The activities of selected Nsp1 mutants on CrPV IRES and $(CAA)_4$-MF β-globin mRNAs are shown in Figure 6, D and E, respectively. Mutants with reduced activity preferentially induced cleavage at the 5′-terminal site on the EMCV IRES mRNA indicating the highest affinity of the nuclease to it, which was proportional to the relative loss of activity (e.g., K11A or R77A vs. K129A or H134A mutants) (Fig. 6A [lanes 3,10], B [lanes 10,11]). Importantly, in toeprinting experiments done without prior phenol extraction, all inactive/low-activity Nsp1 mutants inhibited 48S complex formation on the EMCV IRES (Fig. 6F–H), confirming that they retained ribosomal binding activity. Preferential 5′-terminal cleavage of $(CAA)_4$-MF β-globin mRNA by impaired Nsp1 mutants (Fig. 6E) was consistent with time course data showing that cleavage is sequential and starts from the 5′-terminal site (Fig. 1F). Mapping of the residues important for mRNA cleavage onto the crystal structure of the Nsp1 NTD showed that they formed an essential, mostly positively charged surface (Fig. 6I). The important residues could potentially be involved in the interaction with mRNA, translational components (40S subunits and/or eIF3g), or catalysis of mRNA cleavage per se. Taking into account residues that have established catalytic functions in endonucleases (Yang 2011), we focused on mutating conserved His and Asp/Glu residues that might contribute to Nsp1-induced catalysis. The E91A substitution abrogated cleavage activity (Fig. 6C, lane 8), whereas H13A (Fig. 6A, lane 4), H81A, H83A, H134A (Fig. 6B, lanes 7,8,11), and D75A (Fig. 6C, lane 7) substitutions very strongly impaired but did not abolish Nsp1-induced cleavage.

Inhibition of Nsp1-induced cleavage

Nsp1 is a potential target for inhibition because of its importance for pathogenesis and its sequence and structural conservation. Several chemicals and FDA-approved drugs that could be modified or repurposed as therapeutic SARS-CoV-2 inhibitors have been validated by analysis of binding to Nsp1 (Afsar et al. 2022; Borsatto et al. 2022; Kumar et al. 2022) or by inhibition of its function in cells (Afsar et al. 2022; Kao et al. 2022). Candidate inhibitors include (1) montelukast, a leukotriene receptor antagonist that requires the Nsp1 C-terminal region for binding, modestly impairs SARS-CoV-2 replication, and inhibits Nsp1-mediated cytopathic effects (CPE) (Kumar et al. 2021; Afsar et al. 2022; Kao et al. 2022); (2) artesunate, a derivative of an antimalarial drug that may disrupt Nsp1 structure (Gurung et al. 2022); (3) the tyrosine kinase inhibitor ponatinib and (4) the 21-aminosteroid lipid peroxidation inhibitor tirilazad, which synergize with montelukast in inhibiting Nsp1-mediated CPE (Kao et al. 2022); (5) glycyrrhizic acid (Vankadari et al. 2020); and (6) mitoxantrone dihydrochloride, an anthracenedione that binds to the Nsp1 CTD (Kumar et al. 2022).

We tested the influence of these compounds at 500 and 10 μM concentrations using CrPV IRES mRNA, which requires a minimal set of components for Nsp1-induced cleavage. Only mitoxantrone (Fig. 7A) was active at a low concentration. At 10 μM, it abrogated mRNA cleavage while allowing 40S/IRES complex formation (Fig. 7B, lane 8), and its activity reduced progressively starting from 5 μM (Fig. 7C). Mitoxantrone is FDA-approved for the treatment of multiple sclerosis and several types of cancer. Its best-characterized activity is as a topoisomerase II inhibitor and DNA intercalator (Evison et al. 2016).

Even though montelukast was not active at 10 μM, its inhibition of reverse transcription at 500 μM (Fig. 7B, lanes 5,6) necessitated investigation of its activity at intermediate concentrations. At 100 μM, montelukast abrogated Nsp1-induced cleavage (Fig. 7D), but this concentration was 10 times higher than the inhibitory concentration of mitoxantrone. Thus, our further studies focused on the activity of mitoxantrone.

Mitoxantrone's influence on Nsp1-mediated inhibition of 48S complex formation was assayed using HCV IRES mRNA, on which Nsp1 does not induce cleavage. Mitoxantrone did not impair the ability of Nsp1 to inhibit initiation on this IRES (Fig. 7E, lanes 3,5,7,9) but affected 48S complex formation even in the absence of Nsp1 (Fig. 7E, cf. lanes 2,4,6,8). The inhibitory effect of mitoxantrone on 48S complex formation was more pronounced on $(CAA)_4$-MF β-globin mRNA (Fig. 7F, lanes 2,4).

Mitoxantrone has a planar heterocyclic ring structure with keto groups at the ninth and 10th positions, hydroxy substituents at the fifth and eighth positions, and (hydroxyethylamino)–ethylamino side chains at the first and fourth positions (Fig. 7A). To gain insight into the contribution of structural elements to the inhibition of Nsp1, we evaluated two related anthracenediones: ametantrone and pixantrone (Fig. 7A). Ametantrone lacks hydroxy substituents at the fifth and eighth positions (Zee-Cheng and Cheng 1978); pixantrone also lacks these groups but has a nitrogen heteroatom inserted into the same ring and ethylamino–diethylamino side chains at the first and fourth positions (Menna et al. 2016). Both compounds were more potent inhibitors than mitoxantrone, abrogating Nsp1-induced cleavage of CrPV mRNA at 2.5 μM (Fig. 7G, lanes 13,15).

In conclusion, Nsp1-induced mRNA cleavage can be inhibited specifically while preserving the ability of Nsp1 to inhibit 48S complex formation.

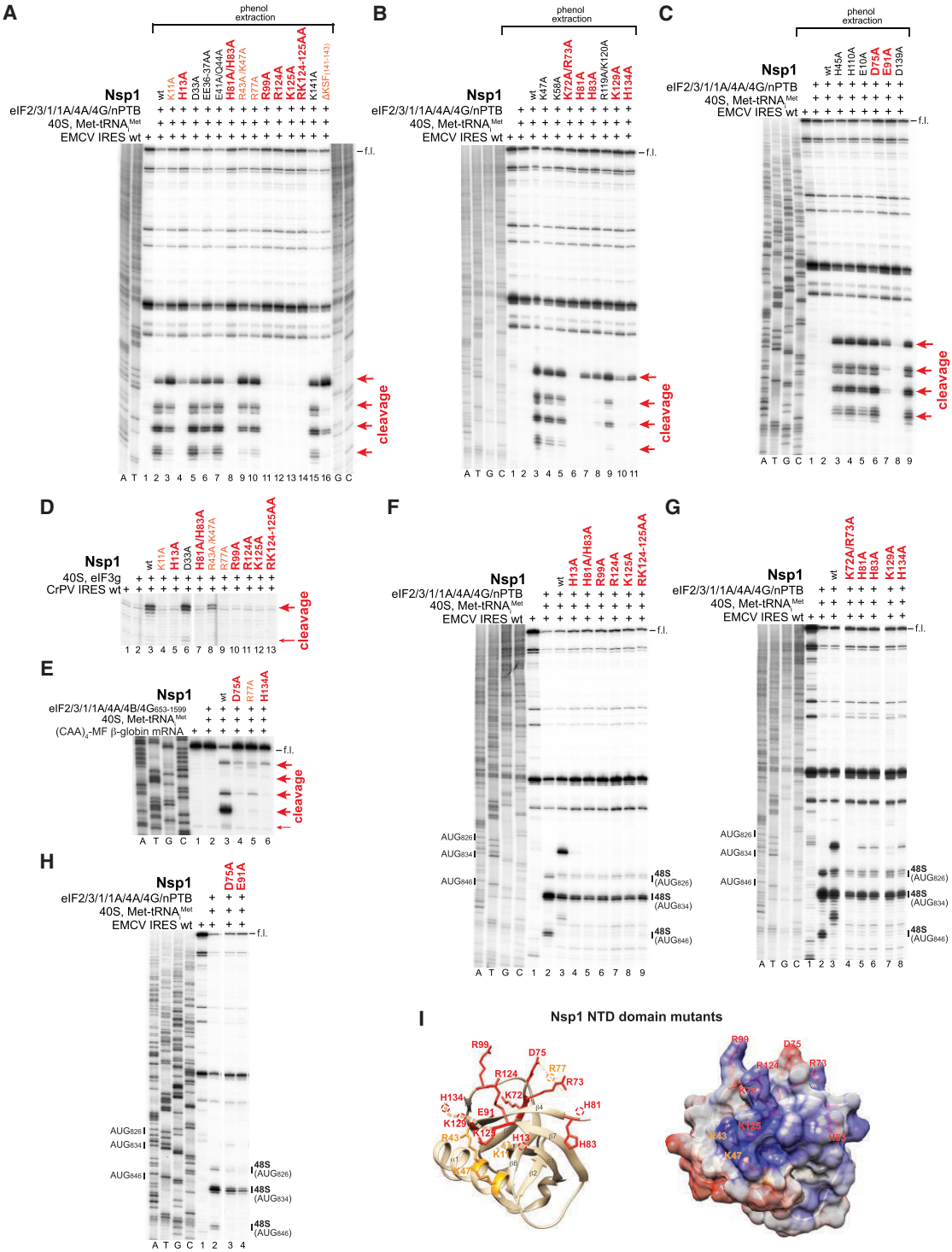

Figure 6. Mutational analysis of SARS-CoV-2 Nsp1. (*A–C*) Cleavage of EMCV IRES mRNA induced by wt and Ala substitution mutant Nsp1s in the presence of the indicated translation components, assayed by primer extension after phenol extraction of mRNA. (*D*,*E*) Cleavage of CrPV IRES (*D*) and (CAA)$_4$-MF β-globin (*E*) mRNAs in the presence of wt and Ala substitution mutant Nsp1s and the indicated translation components, assayed by toeprinting. (*A–E*) Mutations having the strongest effect on Nsp1-induced cleavage in *A–C* are in red, mutations causing a moderate effect are in orange, and mutations that do not affect cleavage are in black. (*F–H*) Inhibition of 48S complex formation on the EMCV IRES mRNA by Nsp1 Ala substitution mutants with the lowest cleavage-inducing activity, assayed by toeprinting. Separation of lanes in *D*, *G*, and *H* by white lines indicates that these parts were juxtaposed from the same gels. (*I*) Ribbon diagram (*left* panel) and surface charge distribution (*right* panel) of the Nsp1 NTD (PDB: 7K3N) in ribbon (*left* panel) and space-filling (*right* panel) representations, annotated to show residues that contribute strongly (red sticks) or moderately (orange sticks) to Nsp1-induced cleavage (as shown in *A–C*).

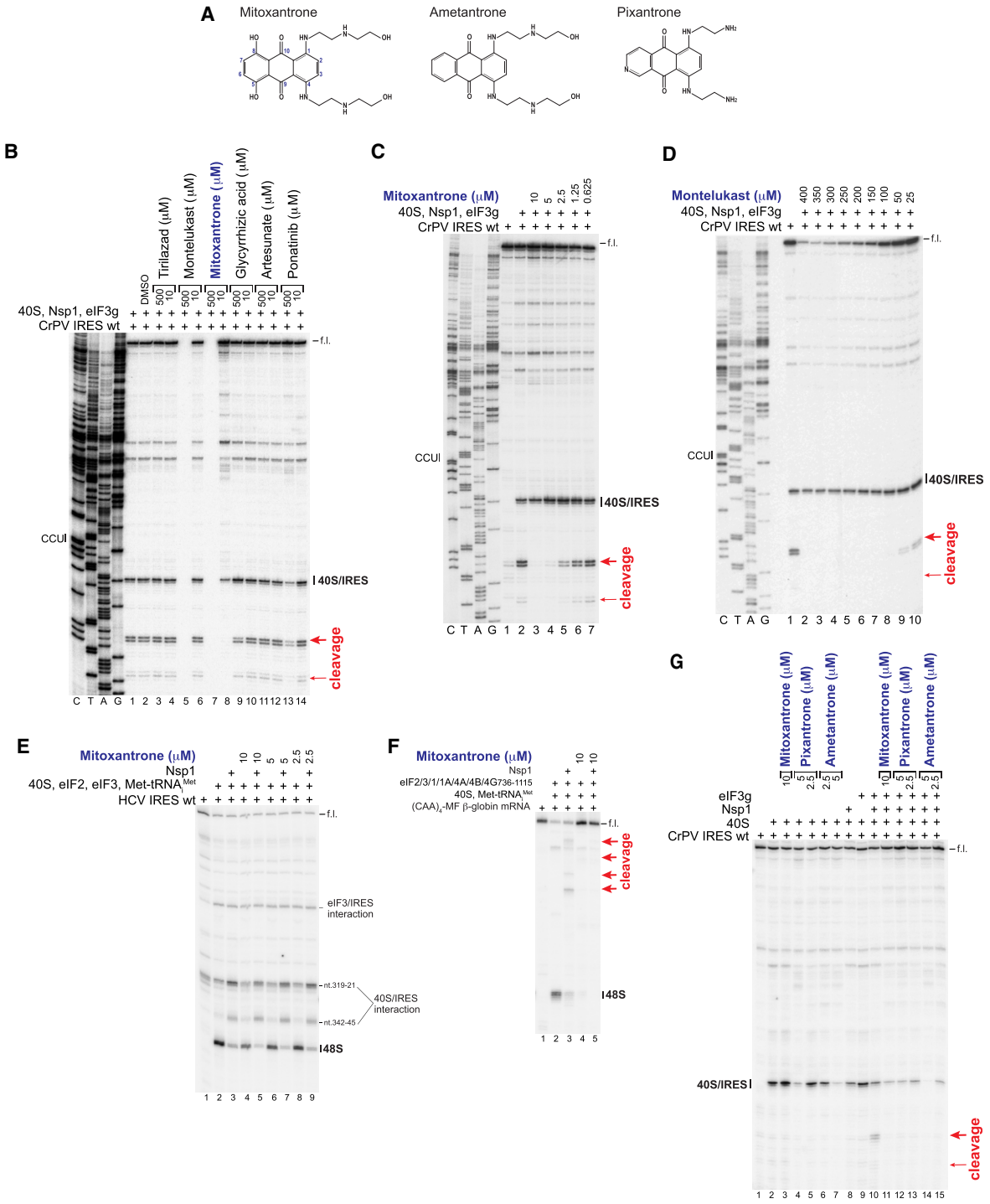

Figure 7. Chemical inhibition of SARS-CoV-2 Nsp1-induced cleavage of mRNA. (*A*) Structures of mitoxantrone, ametantrone, and pixantrone. (*B–G*) The influence of FDA-approved drugs on Nsp1-induced mRNA cleavage and inhibition of 48S complex formation on CrPV IRES (*B–D*,*G*), HCV IRES (*E*), and $(CAA)_4$-MF β-globin (*F*) mRNAs in the presence of the indicated translation components, assayed by toeprinting.

Discussion

To investigate the mechanism of SARS-CoV-2 Nsp1-induced endonucleolytic cleavage of mRNA, we reconstituted this process in vitro on β-globin, EMCV IRES, and CrPV IRES mRNAs that use unrelated mechanisms to initiate translation. Our results argue against the involvement of a putative cellular RNA endonuclease and establish the essential roles of the C-terminal RRM domain of the eIF3g subunit of eIF3 and the Nsp1 NTD

in the cleavage process irrespective of the mode of initiation. Requirements for other initiation factors differed for these three mRNAs, reflecting the distinct initiation mechanisms that they use and specifically the different factor requirements of each for ribosomal attachment.

The Nsp1-induced cleavage of CrPV IRES mRNA required a minimal set of translational components consisting of only a 40S subunit and eIF3g's RRM domain. The cleavage site was located 18 nt downstream from the toeprints corresponding to 40S/IRES complexes. The position of the cleavage site and the ribosomal location of eIF3g's RRM domain at the mRNA entrance (Brito Querido et al. 2020) indicate that Nsp1-induced cleavage takes place on the solvent side of the 40S subunit downstream from the mRNA entrance. Mutational analysis identified a positively charged surface on the Nsp1 NTD and a surface above the mRNA-binding channel on the RRM domain of eIF3g that contain residues essential for cleavage. The key questions concerning the mechanism of cleavage include the exact identity of the nuclease and the individual roles of all components (i.e., the Nsp1 NTD, eIF3g's RRM domain, and the 40S subunit) in this process. Although the intrinsic endonucleolytic activity of SARS-CoV-2 Nsp1 has recently been reported (Tardivat et al. 2023), it was observed only at high Nsp1 concentrations (which may suggest the possibility of contamination) and in a specific buffer lacking monovalent cations. Therefore, it would be premature to conclude that Nsp1 forms a catalytic site entirely on its own rather than in a complex with eIF3g and/or a 40S subunit, particularly because meaningful mRNA cleavage by Nsp1 off the ribosome in translation buffer conditions has not been detected by us (this study) or by others (Kamitani et al. 2009).

A triple substitution of critical residues in the RNP motifs of the RRM domain of *S. cerevisiae* Tif35/eIF3g reduces the processivity of scanning and resumption of scanning by posttermination ribosomes (Cuchalová et al. 2010), suggesting that the RRM domain might interact with the backbone of mRNA outside the entry channel. The key residues in the RNP motifs of eIF3g (i.e., R242 and K280) were also important for Nsp1-mediated cleavage, as were other residues in the same cavity that faces the mRNA-binding channel. Moreover, cross-linking MS analysis of DSSO-cross-linked HEK293T cells overexpressing FLAG-tagged Nsp1 revealed extensive cross-links between the Nsp1 NTD and the residues of the eIF3g RRM domain that are surface-exposed in the 43S complex, indicating that the interaction between Nsp1 and eIF3g, either direct or mRNA-dependent, can occur in the context of 43S ribosomal complexes (Graziadei et al. 2022). The cross-linked Lys residues in the Nsp1 NTD (Graziadei et al. 2022) were located on the same surface as or in close proximity to residues that were essential for Nsp1-induced cleavage. Thus, eIF3g's RRM domain could potentially function to correctly orient the Nsp1 NTD, act as a conduit for mRNA, or even contribute to catalysis if the nuclease catalytic site is formed not by Nsp1 alone but as a composite of Nsp1 and the eIF3g RRM domain. Consistently, there are also several not mutually exclusive possibilities for the role of the essential Nsp1 NTD surface: (1) to interact with eIF3g, (2) to interact with the 40S subunit, and (3) to interact with mRNA and form the nuclease active center. The role of the 40S subunit is likely limited to being a scaffold for the spatial arrangement of the other components.

The Nsp1 NTD and the RRM domain of eIF3g also had essential roles in Nsp1-induced cleavage of the 5′ end-dependent β-globin and EMCV IRES-containing mRNAs; however, in contrast to the CrPV IRES mRNA, cleavage on these mRNAs required additional initiation factors. Thus, cleavage of β-globin mRNA needed group 4 eIFs and intact native eIF3 that mediate ribosomal attachment during 5′ end-dependent initiation, whereas cleavage of the EMCV IRES mRNA additionally required the eIF2 • GTP/Met-tRNA$_i^{Met}$ ternary complex. Ribosomal attachment to this IRES depends on the specific interaction of its JK domain with the central eIF4A-binding domain of eIF4G (Pestova et al. 1996). However, the JK domain is not sufficient for ribosomal attachment to the IRES, and the requirement of the eIF2 ternary complex for Nsp1-mediated cleavage of EMCV IRES mRNA suggests the essential, as yet unidentified role of eIF2 • GTP/Met-tRNA$_i^{Met}$ in ribosomal attachment.

In all cases, we observed several cleavage sites separated by 6–9 nt. However, detection of a single 5′-terminal mRNA fragment during Nsp1-mediated cleavage of cap-labeled β-globin mRNA and the progressive accumulation of shorter 3′-terminal fragments in the time course experiment clearly indicate that cleavage is sequential rather than random and starts from the 5′ end. Consistently, if cleavage was inefficient (e.g., as in the presence of some Nsp1 mutants), it did not have the time/opportunity to progress further than the 5′-terminal sites. The first 5′-terminal cleavage that separates the cap-containing region from the rest of a cellular mRNA, even without its subsequent degradation, would have a profound effect on host protein synthesis.

The question remains whether mRNA dissociates from the 40S subunit after the first cleavage and then rebinds, leading to cleavage at the next downstream site as a result of a separate attachment event, or whether mRNA remains associated with 40S ribosomal complexes, and group 4 eIFs continuously feed it into the nuclease active center. The 6- to 9-nt spacing between cleavage sites suggests that cleavage requires the accommodation of the upstream 5′-terminal six to nine mRNA nucleotides in the nuclease active center. The minor variation in the distance between cleavage sites may be indicative of a small degree of nucleotide specificity of cleavage. Notably, the 5′-terminal cleavage site was located close to the 5′ end of mRNA, and even in conditions of eIF4E–cap interaction during cleavage of native capped β-globin mRNA in the presence of native eIF4F, the first cleavage site was only 7 nt from the cap. Regarding the ribosomal position of the eIF3g RRM domain and its cross-linking to the Nsp1 NTD, it is difficult to reconcile the position of the 5′-terminal cleavage site with the suggested ribosomal position of eIF4E and the proposed slotting mechanism of ribosomal attachment during 5′ end-dependent initiation (Brito Querido et al. 2020) because in this case the 5′-terminal mRNA region would be too far from the hypothetical nuclease active center. On the other

hand, the position of the 5′-terminal cleavage site would be more consistent with a mechanism in which mRNA is threaded into the mRNA-binding channel through its entrance (Kumar et al. 2016). In contrast to CrPV mRNA, no cleavage was observed in the coding region of β-globin mRNA. Strong inhibition of 48S complex formation on β-globin mRNA by wt and mutant Nsp1 indicates that the coexistence of Nsp1 with accommodated mRNA is unique to the CrPV IRES, which does not require the eIF2 • GTP/Met-$tRNA_i^{Met}$ ternary complex and binds to the A site of the 40S subunit.

In the case of the EMCV IRES mRNA, cleavage occurs in regions that are very close to domain L and, during initiation, would most likely be slotted into the mRNA-binding channel. In the presence of Nsp1, this region likely remains on the solvent side of the 40S subunit. Sequence and/or structural features of the region enable two particular areas in it to be independently accommodated in the nuclease active center, yielding cleavages at nucleotides 830–831 and 849–850, respectively. Subsequent downstream cleavage could potentially result from the 5′ end-dependent attachment of truncated mRNAs to mRNA-free 43S complexes. The mechanistic basis for downstream cleavages on the CrPV IRES mRNA is also not clear, and they could also result from 5′ end-dependent attachment of truncated mRNAs to mRNA-free 40S ribosomal complexes.

In conclusion, we identified the essential role of the Nsp1 NTD and the RRM domain of eIF3g in Nsp1-induced cleavage of mRNAs and determined the initiation factor requirements for this process on mRNAs translated by three different initiation mechanisms, thus providing the foundation and the framework for future structural studies of the molecular mechanism of cleavage.

Materials and methods

Plasmid construction; purification of ribosomal subunits, initiation factors, Nsp1, and aminoacyl-tRNA synthetases; preparation of mRNAs and tRNAs; mRNA capping and 3′-labeling; and aminoacylation of tRNAs are described in the Supplemental Material, which also contains detailed protocols for all experimental procedures.

In vitro reconstitution and analysis of Nsp1-induced cleavages

To reconstitute Nsp1-induced cleavage of mRNA, 40S subunits were preincubated with wt or mutant Nsp1 for 10 min at 37°C in buffer A (20 mM Tris at pH 7.5, 2 mM dithiothreitol, 0.25 mM spermidine, 2.5 mM, 1 mM ATP, 0.5 mM GTP), after which reaction mixtures were supplemented with $(CAA)_4$-MF β-globin, native β-globin, wt or mutant EMCV IRES, wt or mutant CrPV IRES, or wt HCV IRES mRNAs and the indicated combinations of eIF2; native or mutant eIF3, eIF1, eIF1A, eIF4A, eIF4B, $eIF4G_{653–1599}$, or $eIF4G_{736–1115}$; eIF4F; DHX29; wt or mutant eIF3g; nPTB; and Met-$tRNA_i^{Met}$. After that, incubation continued for an additional 15 min, except for the time course experiments in which aliquots were removed from the reaction mixtures at the indicated time points. To investigate the influence of tirilizad, montelukast, artesunate, ponatinib, mitoxantrone, glycyrrhizic acid, ametantrone (Cayman Chemical), and pixantrone maleate (Selleck Chemicals) on Nsp1 activity, each drug was dissolved in DMSO and added to buffer A to reach the desired concentration.

To investigate the influence of Nsp1 on mRNA in assembled 80S complexes and on their ability to undergo elongation, 80S initiation complexes were formed on $(CAA)_4$-MF β-globin by incubating mRNA with 40S subunits, eIF2, eIF3, eIF1, eIF1A, eIF4A, $eIF4G_{736–1115}$, and Met-$tRNA_i^{Met}$ in buffer A for 15 min at 37°C, after which reaction mixtures were supplemented with 60S subunits, eIF5, and eIF5B, and incubation continued for another 15 min. 80S complexes were then incubated for 15 min with the indicated combinations of Nsp1, eEF1H, eEF2, and Phe-$tRNA^{Phe}$.

To detect cleavage of unlabeled mRNAs, reaction mixtures were analyzed by toeprinting or by primer extension after phenol extraction and ethanol precipitation using AMV RT and ^{32}P-labeled primer (Pisarev et al. 2007). cDNA products were resolved on 6% sequencing gel and analyzed by phosphorimager. In the case of ^{32}P-labeled mRNAs, after incubation with Nsp1 and translational components, mRNA was subjected to electrophoresis on 6% sequencing gel and analyzed by phosphorimager.

Competing interest statement

The authors declare no competing interests.

Acknowledgments

We thank Andrew Tcherepanov for expert technical assistance. This work was supported by National Institutes of Health grants GM122602 (to T.V.P.) and AI166944 to (T.V.P. and C.U.T.H.).

Author contributions: I.S.A., Y.A., and A.M. performed all experiments. T.V.P., C.U.T.H., I.S.A., Y.A., and A.M. designed experiments and interpreted data. T.V.P. and C.U.T.H. wrote the manuscript with input from all authors.

References

Abaeva IS, Marintchev A, Pisareva VP, Hellen CUT, Pestova TV. 2011. Bypassing of stems versus linear base-by-base inspection of mammalian mRNAs during ribosomal scanning. *EMBO J.* **30:** 115–129. doi:10.1038/emboj.2010.302

Abernathy E, Glaunsinger B. 2015. Emerging roles for RNA degradation in viral replication and antiviral defense. *Virology* **479-480:** 600–608. doi:10.1016/j.virol.2015.02.007

Afsar M, Narayan R, Akhtar MN, Das D, Rahil H, Nagaraj SK, Eswarappa SM, Tripathi S, Hussain T. 2022. Drug targeting Nsp1-ribosomal complex shows antiviral activity against SARS-CoV-2. *Elife* **11:** e74877. doi:10.7554/eLife.74877

Almeida MS, Johnson MA, Herrmann T, Geralt M, Wüthrich K. 2007. Novel β-barrel fold in the nuclear magnetic resonance structure of the replicase nonstructural protein 1 from the severe acute respiratory syndrome coronavirus. *J Virol* **81:** 3151–3161. doi:10.1128/JVI.01939-06

Asano K, Phan L, Anderson J, Hinnebusch AG. 1998. Complex formation by all five homologues of mammalian translation initiation factor 3 subunits from yeast *Saccharomyces cerevisiae*. *J Biol Chem* **273:** 18573–18585. doi:10.1074/jbc.273.29.18573

Banerjee AK, Blanco MR, Bruce EA, Honson DD, Chen LM, Chow A, Bhat P, Ollikainen N, Quinodoz SA, Loney C, et al. 2020. SARS-CoV-2 disrupts splicing, translation, and protein trafficking to suppress host defenses. *Cell* **183:** 1325–1339.e21. doi:10.1016/j.cell.2020.10.004

Borsatto A, Akkad O, Galdadas I, Ma S, Damfo S, Haider S, Kozielski F, Estarellas C, Gervasio FL. 2022. Revealing druggable cryptic pockets in the Nsp-1 of SARS-CoV-2 and other β-coronaviruses by simulations and crystallography. *Elife* **11:** e81167. doi:10.7554/eLife.81167

Brito Querido J, Sokabe M, Kraatz S, Gordiyenko Y, Skehel JM, Fraser CS, Ramakrishnan V. 2020. Structure of a human 48*S* translational initiation complex. *Science* **369:** 1220–1227. doi:10.1126/science.aba4904

Burgess HM, Vink EI, Mohr I. 2022. Minding the message: tactics controlling RNA decay, modification, and translation in virus-infected cells. *Genes Dev* **36:** 108–132. doi:10.1101/gad.349276.121

Clark LK, Green TJ, Petit CM. 2021. Structure of nonstructural protein 1 from SARS-CoV-2. *J Virol* **95:** e02019-20.

Costantino D, Kieft JS. 2005. A preformed compact ribosome-binding domain in the cricket paralysis-like virus IRES RNAs. *RNA* **11:** 332–343. doi:10.1261/rna.7184705

Costantino DA, Pfingsten JS, Rambo RP, Kieft JS. 2008. tRNA–mRNA mimicry drives translation initiation from a viral IRES. *Nat Struct Mol Biol* **15:** 57–64. doi:10.1038/nsmb1351

Cuchalová L, Kouba T, Herrmannová A, Dányi I, Chiu WL, Valášek L. 2010. The RNA recognition motif of eukaryotic translation initiation factor 3g (eIF3g) is required for resumption of scanning of posttermination ribosomes for reinitiation on *GCN4* and together with eIF3i stimulates linear scanning. *Mol Cell Biol* **30:** 4671–4686. doi:10.1128/MCB.00430-10

des Georges A, Dhote V, Kuhn L, Hellen CU, Pestova TV, Frank J, Hashem Y. 2015. Structure of mammalian eIF3 in the context of the 43S preinitiation complex. *Nature* **525:** 491–495. doi:10.1038/nature14891

Evison BJ, Sleebs BE, Watson KG, Phillips DR, Cutts SM. 2016. Mitoxantrone, more than just another topoisomerase II poison. *Med Res Rev* **36:** 248–299. doi:10.1002/med.21364

Fernández IS, Bai XC, Murshudov G, Scheres SH, Ramakrishnan V. 2014. Initiation of translation by cricket paralysis virus IRES requires its translocation in the ribosome. *Cell* **157:** 823–831. doi:10.1016/j.cell.2014.04.015

Finkel Y, Gluck A, Nachshon A, Winkler R, Fisher T, Rozman B, Mizrahi O, Lubelsky Y, Zuckerman B, Slobodin B, et al. 2021. SARS-CoV-2 uses a multipronged strategy to impede host protein synthesis. *Nature* **594:** 240–245. doi:10.1038/s41586-021-03610-3

Fisher T, Gluck A, Narayanan K, Kuroda M, Nachshon A, Hsu JC, Halfmann PJ, Yahalom-Ronen Y, Tamir H, Finkel Y, et al. 2022. Parsing the role of Nsp1 in SARS-CoV-2 infection. *Cell Rep* **39:** 110954. doi:10.1016/j.celrep.2022.110954

Gaglia MM, Covarrubias S, Wong W, Glaunsinger BA. 2012. A common strategy for host RNA degradation by divergent viruses. *J Virol* **86:** 9527–9530. doi:10.1128/JVI.01230-12

Graziadei A, Schildhauer F, Spahn C, Kraushar M, Rappsilber J. 2022. SARS-CoV-2 Nsp1 N-terminal and linker regions as a platform for host translational shutoff. bioRxiv. doi:10.1101/2022.02.10.479924

Gurung AB, Ali MA, Lee J, Farah MA, Al-Anazi KM, Al-Hemaid F. 2022. Artesunate induces substantial topological alterations in the SARS-CoV-2 Nsp1 protein structure. *J King Saud Univ Sci* **34:** 101810. doi:10.1016/j.jksus.2021.101810

Hashem Y, des Georges A, Dhote V, Langlois R, Liao HY, Grassucci RA, Hellen CU, Pestova TV, Frank J. 2013a. Structure of the mammalian ribosomal 43S preinitiation complex bound to the scanning factor DHX29. *Cell* **153:** 1108–1119. doi:10.1016/j.cell.2013.04.036

Hashem Y, des Georges A, Dhote V, Langlois R, Liao HY, Grassucci RA, Pestova TV, Hellen CU, Frank J. 2013b. Hepatitis-C-virus-like internal ribosome entry sites displace eIF3 to gain access to the 40S subunit. *Nature* **503:** 539–543. doi:10.1038/nature12658

Herrmannová A, Daujotytė D, Yang JC, Cuchalová L, Gorrec F, Wagner S, Dányi I, Lukavsky PJ, Valášek LS. 2012. Structural analysis of an eIF3 subcomplex reveals conserved interactions required for a stable and proper translation pre-initiation complex assembly. *Nucleic Acids Res* **40:** 2294–2311. doi:10.1093/nar/gkr765

Huang C, Lokugamage KG, Rozovics JM, Narayanan K, Semler BL, Makino S. 2011. SARS coronavirus nsp1 protein induces template-dependent endonucleolytic cleavage of mRNAs: viral mRNAs are resistant to nsp1-induced RNA cleavage. *PLoS Pathog* **7:** e1002433. doi:10.1371/journal.ppat.1002433

Hsu JC-C, Laurent-Rolle M, Pawlak JB, Wilen CB, Cresswell P. 2021. Translational shutdown and evasion of the innate immune response by SARS-CoV-2 NSP14 protein. *Proc Natl Acad Sci* **118:** e210116118.

Kamitani W, Narayanan K, Huang C, Lokugamage K, Ikegami T, Ito N, Kubo H, Makino S. 2006. Severe acute respiratory syndrome coronavirus nsp1 protein suppresses host gene expression by promoting host mRNA degradation. *Proc Natl Acad Sci* **103:** 12885–12890. doi:10.1073/pnas.0603144103

Kamitani W, Huang C, Narayanan K, Lokugamage KG, Makino S. 2009. A two-pronged strategy to suppress host protein synthesis by SARS coronavirus Nsp1 protein. *Nat Struct Mol Biol* **16:** 1134–1140. doi:10.1038/nsmb.1680

Kao HT, Orry A, Palfreyman MG, Porton B. 2022. Synergistic interactions of repurposed drugs that inhibit Nsp1, a major virulence factor for COVID-19. *Sci Rep* **12:** 10174. doi:10.1038/s41598-022-14194-x

Kolupaeva VG, Lomakin IB, Pestova TV, Hellen CUT. 2003. Eukaryotic initiation factors 4G and 4A mediate conformational changes downstream of the initiation codon of the encephalomyocarditis virus internal ribosomal entry site. *Mol Cell Biol* **23:** 687–698. doi:10.1128/MCB.23.2.687-698.2003

Kumar P, Hellen CU, Pestova TV. 2016. Toward the mechanism of eIF4F-mediated ribosomal attachment to mammalian capped mRNAs. *Genes Dev* **30:** 1573–1588. doi:10.1101/gad.282418.116

Kumar S, Singh B, Kumari P, Kumar PV, Agnihotri G, Khan S, Beuria TK, Syed GH, Dixit A. 2021. Identification of multipotent drugs for COVID-19 therapeutics with the evaluation of their SARS-CoV2 inhibitory activity. *Comput Struct Biotechnol J* **19:** 1998–2017. doi:10.1016/j.csbj.2021.04.014

Kumar P, Bhardwaj T, Giri R. 2022. Mitoxantrone dihydrochloride, an FDA approved drug, binds with SARS-CoV-2 Nsp1 C-terminal. *RSC Adv* **12:** 5648–5655. doi:10.1039/D1RA07434B

Lapointe CP, Grosely R, Johnson AG, Wang J, Fernández IS, Puglisi JD. 2021. Dynamic competition between SARS-CoV-2 NSP1 and mRNA on the human ribosome inhibits translation initiation. *Proc Natl Acad Sci* **118:** e2017715118. doi:10.1073/pnas.2017715118

Lokugamage G, Narayanan K, Huang C, Makino S. 2012. Severe acute respiratory syndrome coronavirus protein nsp1 is a novel eukaryotic translation inhibitor that represses multiple steps of translation initiation. *J Virol* **86:** 13598–13608. doi:10.1128/JVI.01958-12

Lomakin IB, Hellen CU, Pestova TV. 2000. Physical association of eukaryotic initiation factor 4G (eIF4G) with eIF4A strongly enhances binding of eIF4G to the internal ribosomal entry site of encephalomyocarditis virus and is required for internal initiation of translation. *Mol Cell Biol* **20:** 6019–6029. doi:10.1128/MCB.20.16.6019-6029.2000

Mendez AS, Ly M, González-Sánchez AM, Hartenian E, Ingolia NT, Cate JH, Glaunsinger BA. 2021. The N-terminal domain of SARS-CoV-2 nsp1 plays key roles in suppression of cellular gene expression and preservation of viral gene expression. *Cell Rep* **37:** 109841. doi:10.1016/j.celrep.2021.109841

Menna P, Salvatorelli E, Minotti G. 2016. Rethinking drugs from chemistry to therapeutic opportunities: pixantrone beyond anthracyclines. *Chem Res Toxicol* **29:** 1270–1278. doi:10.1021/acs.chemrestox.6b00190

Minkoff JM, tenOever B. 2023. Innate immune evasion strategies of SARS-CoV-2. *Nat Rev Microbiol* **21:** 178–194.

Muhs M, Yamamoto H, Ismer J, Takaku H, Nashimoto M, Uchiumi T, Nakashima N, Mielke T, Hildebrand PW, Nierhaus KH, et al. 2011. Structural basis for the binding of IRES RNAs to the head of the ribosomal 40S subunit. *Nucleic Acids Res* **39:** 5264–5275. doi:10.1093/nar/gkr114

Muto Y, Yokoyama S. 2012. Structural insight into RNA recognition motifs: versatile molecular Lego building blocks for biological systems. *Wiley Interdiscip Rev RNA* **3:** 229–246. doi:10.1002/wrna.1107

Nakagawa K, Makino S. 2021. Mechanisms of coronavirus Nsp1-mediated control of host and viral gene expression. *Cells* **10:** 300. doi:10.3390/cells10020300

Narayanan K, Huang C, Lokugamage K, Kamitani W, Ikegami T, Tseng CT, Makino S. 2008. Severe acute respiratory syndrome coronavirus nsp1 suppresses host gene expression, including that of type I interferon, in infected cells. *J Virol* **82:** 4471–4479. doi:10.1128/JVI.02472-07

Pestova TV, Kolupaeva VG. 2002. The roles of individual eukaryotic translation initiation factors in ribosomal scanning and initiation codon selection. *Genes Dev* **16:** 2906–2922. doi:10.1101/gad.1020902

Pestova TV, Shatsky IN, Hellen CU. 1996. Functional dissection of eukaryotic initiation factor 4F: the 4A subunit and the central domain of the 4G subunit are sufficient to mediate internal entry of 43S preinitiation complexes. *Mol Cell Biol* **16:** 6870–6878. doi:10.1128/MCB.16.12.6870

Pestova TV, Shatsky IN, Fletcher SP, Jackson RJ, Hellen CU. 1998. A prokaryotic-like mode of cytoplasmic eukaryotic ribosome binding to the initiation codon during internal translation initiation of hepatitis C and classical swine fever virus RNAs. *Genes Dev* **12:** 67–83. doi:10.1101/gad.12.1.67

Pestova TV, Lomakin IB, Hellen CU. 2004. Position of the CrPV IRES on the 40S subunit and factor dependence of IRES/80S ribosome assembly. *EMBO Rep* **5:** 906–913. doi:10.1038/sj.embor.7400240

Pisarev AV, Unbehaun A, Hellen CU, Pestova TV. 2007. Assembly and analysis of eukaryotic translation initiation complexes. *Methods Enzymol* **430:** 147–177. doi:10.1016/S0076-6879(07)30007-4

Schubert K, Karousis ED, Jomaa A, Scaiola A, Echeverria B, Gurzeler LA, Leibundgut M, Thiel V, Mühlemann O, Ban N. 2020. SARS-CoV-2 Nsp1 binds the ribosomal mRNA channel to inhibit translation. *Nat Struct Mol Biol* **27:** 959–966. doi:10.1038/s41594-020-0511-8

Semper C, Watanabe N, Savchenko A. 2021. Structural characterization of nonstructural protein 1 from SARS-CoV-2. *iScience* **24:** 101903. doi:10.1016/j.isci.2020.101903

Shen Z, Wang G, Yang Y, Shi J, Fang L, Li F, Xiao S, Fu ZF, Peng G. 2019. A conserved region of nonstructural protein 1 from α-coronaviruses inhibits host gene expression and is critical for viral virulence. *J Biol Chem* **294:** 13606–13618. doi:10.1074/jbc.RA119.009713

Snijder EJ, Bredenbeek PJ, Dobbe JC, Thiel V, Ziebuhr J, Poon LL, Guan Y, Rozanov M, Spaan WJ, Gorbalenya AE. 2003. Unique and conserved features of genome and proteome of SARS-coronavirus, an early split-off from the coronavirus group 2 lineage. *J Mol Biol* **331:** 991–1004. doi:10.1016/S0022-2836(03)00865-9

Tardivat Y, Sosnowski P, Tidu A, Westhof E, Eriani G, Martin F. 2023. SARS-CoV-2 NSP1 induces mRNA cleavages on the ribosome. *Nucleic Acids Res* **51:** 8677–8690. doi:10.1093/nar/gkad627

Thoms M, Buschauer R, Ameismeier M, Koepke L, Denk T, Hirschenberger M, Kratzat H, Hayn M, Mackens-Kiani T, Cheng J, et al. 2020. Structural basis for translational shutdown and immune evasion by the Nsp1 protein of SARS-CoV-2. *Science* **369:** 1249–1255. doi:10.1126/science.abc8665

Vankadari N, Jeyasankar NN, Lopes WJ. 2020. Structure of the SARS-CoV-2 Nsp1/5′-untranslated region complex and implications for potential therapeutic targets, a vaccine, and virulence. *J Phys Chem Lett* **11:** 9659–9668. doi:10.1021/acs.jpclett.0c02818

Wang Y, Kirkpatrick J, Lage SZ, Carlomagno T. 2023. Structural insights into the activity regulation of full-length non-structural protein 1 from SARS-CoV-2. *Structure* **31:** 128–137.e5. doi:10.1016/j.str.2022.12.006

Wathelet MG, Orr M, Frieman MB, Baric RS. 2007. Severe acute respiratory syndrome coronavirus evades antiviral signaling: role of Nsp1 and rational design of an attenuated strain. *J Virol* **81:** 11620–11633. doi:10.1128/JVI.00702-07

Wilson JE, Pestova TV, Hellen CU, Sarnow P. 2000. Initiation of protein synthesis from the A site of the ribosome. *Cell* **102:** 511–520. doi:10.1016/S0092-8674(00)00055-6

Yang W. 2011. Nucleases: diversity of structure, function and mechanism. *Q Rev Biophys* **44:** 1–93. doi:10.1017/S0033583510000181

Yuan S, Peng L, Park JJ, Hu Y, Devarkar SC, Dong MB, Shen Q, Wu S, Chen S, Lomakin IB, et al. 2020. Nonstructural protein 1 of SARS-CoV-2 is a potent pathogenicity factor redirecting host protein synthesis machinery toward viral RNA. *Mol Cell* **80:** 1055–1066.e6. doi:10.1016/j.molcel.2020.10.034

Zee-Cheng RK, Cheng CC. 1978. Antineoplastic agents. Structure-activity relationship study of bis(substituted aminoalkylamino)anthraquinones. *J Med Chem* **21:** 291–294. doi:10.1021/jm00201a012

Zhang K, Miorin L, Makio T, Dehghan I, Gao S, Xie Y, Zhong H, Esparza M, Kehrer T, Kumar A, et al. 2021. Nsp1 protein of SARS-CoV-2 disrupts the mRNA export machinery to inhibit host gene expression. *Sci Adv* **7:** eabe7386. doi:10.1126/sciadv.abe7386

Züst R, Cervantes-Barragán L, Kuri T, Blakqori G, Weber F, Ludewig B, Thiel V. 2007. Coronavirus non-structural protein 1 is a major pathogenicity factor: implications for the rational design of coronavirus vaccines. *PLoS Pathog* **3:** e109. doi:10.1371/journal.ppat.0030109